Supporting Information

SO_2-Tolerant Electrochemical CO_2 Capture and $NaHCO_3$ Conversion Enabled by Saline Water Electrolysis

Tengxiu Tu[ab], Xinyuan Zhang[a], Yijin Wu[ac], Zhixian Mao[ab], Jifang Zhang[a], Jiapeng Ji[f], Lei Xing[d]*, Jian Kang[a], Shan Chen[a], Porun Liu[e], Haimin Zhang[ab], Huajie Yin[ab]*, Huijun Zhao[a]*

[a] Centre for Resource Innovation, Anhui Key Laboratory of Nanomaterials and Nanotechnology, Institute of Solid State Physics, Hefei Institutes of Physical Science, Chinese Academy of Sciences, Hefei, Anhui 230031, China.

[b]University of Science and Technology of China, Hefei, Anhui 230026, China.

[c]Hunan Engineering Research Center for monitoring and treatment of heavy metals pollution in the upper reaches of XiangJiang River, Key Laboratory of Functional Metal-Organic Compounds of Hunan Province, College of Chemistry and Material Science, Hengyang Normal University, Hengyang, 421001, China.

[d]School of Chemistry and Chemical Engineering, Faculty of Engineering and Physical Sciences, University of Surrey, Guildford GU2 7XH, United Kingdom.

[e]Centre for Catalysis and Clean Energy, School of Environment and Science, Griffith University Gold Coast Campus, Queensland, 4222, Australia.

[f]Shenzhen Key Laboratory of Energy Materials for Carbon Neutrality, Institute of Technology for Carbon Neutrality, Shenzhen Institute of Advanced Technology, Chinese Academy of Sciences, Shenzhen, Guangdong, 518055, China.

*Corresponding authors: yinhj@issp.ac.cn, l.xing@surrey.ac.uk and hjzhao@issp.ac.cn

Table of contents

Supplementary Text:

Chemicals and Materials

Sodium chloride (NaCl, ≥ 99.5%) and hydrochloric acid (HCl, ≥ 99.0%) were purchased from Sinopharm Chemical Reagent Co., Ltd., Cobaltous nitrate hexahydrate ($Co(NO_3)_2 \cdot 6H_2O$, 99%) was purchased from Shanghai Aladdin Biochemical Technology Co., Ltd., Ruthenium(III) chloride trihydrate ($RuCl_3 \cdot 3H_2O$, 98%) was purchased from Shanghai Macklin Biochemical Co., Ltd. Pt/C (20 wt%), and RuO_2 (99.9%) were bought from Sigma-Aldrich. All chemicals were used as received without further purification, and ultrapure water (18 MΩ·cm) was used throughout the experiments. A commercialized dimensionally stable anode (DSA) was supplied by Suzhou Sure Industrial Technology Co., Ltd.

Material Characterization

Powder X-ray diffraction (XRD) patterns were collected on a Philips X'Pert Pro diffractometer using Cu Kα radiation (λ = 1.5418 Å) operated at 40 kV and 40 mA. Scanning electron microscopy (SEM) images were acquired on a Hitachi SU8020 at an accelerating voltage of 10.0 kV. Aberration-corrected high-angle annular dark-field scanning transmission electron microscopy (AC-HAADF-STEM) was performed on a JEOL NEOARM microscope (Anhui University) at 200 kV. The Ru loading was determined by inductively coupled plasma-optical emission spectrometry (ICP-OES) (Thermo Fisher Scientific, USA). Ru K-edge X-ray absorption spectra (XAS) were measured at the hard X-ray spectroscopy beamline of the Shanghai Synchrotron Radiation Facility (SSRF). Extended X-ray absorption fine structure (EXAFS) fitting employed an S_0^2 value obtained by modeling a reference Ru foil (K-edge at 22,117 eV). Data processing and fitting were carried out with the Demeter package (Athena and Artemis)[1].

Electrochemical Tests of HER Performance

A three-electrode configuration was employed in an H-type cell to physically separate the working and counter electrodes; the reference electrode was placed in the working-electrode compartment. The two compartments were divided by a Nafion 117 membrane (DuPont). Prior to use, the membrane was pretreated in 5% H_2O_2 at 60°C for 1 h. The electrocatalytic HER activity in 1.0 M NaCl (pH = 7.04) was evaluated by linear sweep voltammetry (LSV, scan rate

5 mV s^{-1}). All potentials were converted to the reversible hydrogen electrode (RHE) scale using: *E*(versus RHE) = *E*(Ag/AgCl) + 0.197 + 0.0592×pH. The polarization curves were recorded with 95% iR compensation.

Product Analysis of CO_2 Conversion

After each recycling electrolysis run, dissolved products ($NaHCO_3$ and/or Na_2CO_3) in the catholyte were quantified by acid titration. Briefly, 10 mL of the collected catholyte was titrated with 0.1 M HCl, while continuously monitoring pH with a calibrated pH meter (Mettler Toledo FE28-Standard). The titrant was added dropwise, and two equivalence points were recorded from the pH–volume curve: (1) First endpoint: pH = 8.30, corresponding to neutralization of free NaOH (if present) and the first stage of Na_2CO_3 neutralization ($Na_2CO_3 \rightarrow NaHCO_3$). (2) Second endpoint: pH = 3.90, corresponding to complete neutralization of $NaHCO_3$ ($NaHCO_3 \rightarrow CO_2 + H_2O$). V_1 is the volumes of HCl from start to the first end point (pH =8.30). V_2 is the volumes of HCl from the first end point to the second end point (pH =3.90). The (bi)carbonate concentration is then calculated as below:

$V_1 > V_2$, this indicates that there is excess NaOH in the solution. The difference ($V_1 - V_2$) corresponds to the volume of HCl required to neutralize NaOH.

$$Concentration\ of\ NaOH = \frac{(V_1 - V_2) \times c}{V}$$

$$Concentration\ of\ Na_2CO_3 = \frac{V_2 \times c}{V}$$

$V_1 = V_2$, this indicates that all the NaOH are consumed and only Na_2CO_3 exist inside the liquid samples.

$$Concentration\ of\ Na_2CO_3 = \frac{V_1 \times c}{V}$$

$V_1 < V_2$, this indicates both Na_2CO_3 and $NaHCO_3$ exist inside the liquid samples.

$$Concentration\ of\ Na_2CO_3 = \frac{V_1 \times c}{V}$$

$$Concentration\ of\ NaHCO_3 = \frac{(V_2 - V_1) \times c}{V}$$

where *c* is the concentration of the HCl solution used, and V is the volume of the sample titrated.

Capture Efficiency for CO_2 Capture

The CO_2 capture efficiency (CE) quantifies the fraction of CO_2 removed from the feed gas to evaluate the net CO_2 capture capacity of the system, calculated from the inlet/outlet CO_2 volume fractions and volumetric flow rates:

$$CE = \frac{\chi_{inlet} \times v_{inlet} - \chi_{outlet} \times v_{outlet}}{\chi_{inlet} \times v_{outlet}} \times 100\%$$

where χ_{inlet} and χ_{outlet} are the CO_2 volume fractions in the inlet and outlet gas streams, respectively, and ν_{intlet} and ν_{outlet} are the corresponding volumetric flow rates. **Note:** If the total flow rate is effectively constant across the absorber (i.e., $\nu_{intlet} \approx \nu_{outlet}$), the expression simplifies to:

$$CE \approx (1 - \frac{\chi_{outlet}}{\chi_{inlet}}) \times 100\%$$

CO_2 Conversion Efficiency

The conversion efficiency, CE′, is defined as the fraction of inlet CO_2 that is converted to (bi)carbonate in the electrolyte. It is calculated from the titrated product concentration and the inlet gas flow:

$$CE' = \frac{m \times V_e \times V_{mol}}{\chi_{inlet} \times v_{inlet} \times t} \times 100\%$$

where m is the molar concentration of the product determined by the acid titration method, V_e is the electrolyte volume, V_{mol} is the mole volume of an ideal gas at room temperature, χ_{inlet} is the CO_2 volume fraction in the inlet flue gas, ν_{intlet} is the gas flow rate of inlet, and t is the reaction time.

Formation Rate for (Bi)carbonate Produce

The (bi)carbonate formation rate (N) is calculated by the following formula:

$$N = \frac{m \times V_e}{A \times t}$$

where m is the molar concentration of the product determined by the acid titration method, V_e is the volume of the electrolyte, A is the electrode area, and t is the reaction time.

Faradaic Efficiency for (Bi)carbonate Produce

The Faradaic efficiency (FE) quantifies the fraction of electrons that form (bi)carbonate products during CO_2 capture and conversion. For a given product, FE is calculated as:

$$FE = \frac{n \times F \times m \times V_e}{I \times t} \times 100\%$$

where n is the number of electrons involved (n = 1 for bicarbonate case and n = 2 for carbonate case), F is Faraday constant (96,485C mol^{-1}), m is the molar concentration of the product determined by the acid titration method, V_e is the volume of the electrolyte, I is the applied current, and t is the reaction time.

COMSOL Numerical Simulation

The multiphysics approach combining the Secondary Current Distribution and Transport of Diluted Species interfaces were used to simulate the flow field distribution, mass transfer in a serpentine flow channel, and the electrochemical reactions within the catalyst layer. The computational domain consists of a serpentine channel through which a mixture of CO_2 and water is introduced. To facilitate convergence, the fluid is assumed to be a homogeneous single-phase medium, flow regime is characterized as laminar flow, determined based on the Reynolds number (Re ≈ 1500). Moreover, the channel region is discretized using a default regular mesh, with a linearly distributed swept mesh along the depth direction. The gas diffusion electrode is meshed with free triangular elements, also employing a linearly swept mesh in the depth direction. A boundary layer mesh consisting of two layers is applied at the fluid-solid interfaces, with a stretch factor of 1.3 and a thickness adjustment factor of 2. To ensure model convergence, conventional mesh settings were adopted for the simulations (Fig. S1).

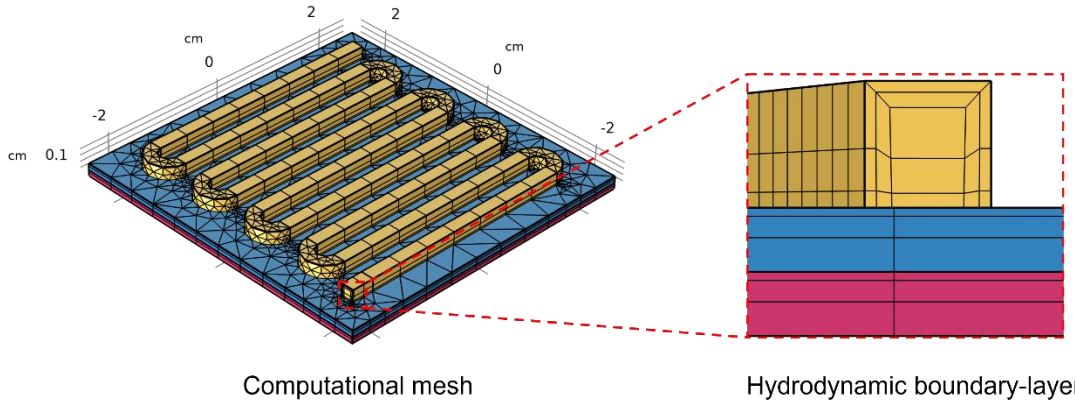

Fig. S1 The overlay of the computational mesh and hydrodynamic boundary-layer. A progressively growing prism layer is used to mesh the near-wall region of the channel.

The numerical simulation was conducted using finite element analysis in COMSOL Multiphysics 6.2, coupling the Nernst-Planck equations in an aqueous electrolyte with laminar

flow in a default stationary solver. Bulk equilibrium reactions were implemented as pointwise rate laws of the form:

$$\frac{dc_i}{dt} = \sum_j \left(k^*j, \rightarrow \prod_i c_i^{vi} - k^*j, \leftarrow \prod_i c_i^{vi} \right) \qquad (S1)$$

c_i represents the concentration of a given species, k*$j\leftrightarrow$ are the forward and reverse rate constants for a given equilibrium reaction accounting for deviations from ideal activity, and v represents the corresponding positive stoichiometric coefficient. Equilibrium reactions and rate constants are tabulated below, as formulated by Zeebe[2] (assuming T=25°C, P=1 bar, and NaCl concentration = 1.0 M):

Table S1: Bulk reaction equilibrium coefficients and rate constants.

Reaction	pK*	K*→	K*←
$CO_2 + H_2O \leftrightharpoons HCO_3^- + H^+$	6.49	3.90×10^{-3} [s^{-1}]	2.58×10^{4} [$M^{-1}\,s^{-1}$]
$CO_2 + OH^- \rightleftharpoons HCO_3^-$	/	3.91×10^{3} [$M^{-1}\,s^{-1}$]	1.76×10^{-4} [s^{-1}]
$CO_3^{2-} + H^+ \rightleftharpoons HCO_3^-$	9.92	4.83×10^{10} [$M^{-1}\,s^{-1}$]	59.44 [s^{-1}]
$HCO_3^- + OH^- \rightleftharpoons CO_3^{2-} + H_2O$	/	5.79×10^{6} [$M^{-1}\,s^{-1}$]	3.06×10^{5} [s^{-1}]
$H_2O \rightleftharpoons OH^- + H^+$	13.19	1.45×10^{3} [$M\,s^{-1}$]	2.23×10^{10} [$M\,s^{-1}$]

Nominal reaction timescales for DIC interconversion calculated by Zeebe is order 10^{-7}s for interconversion between carbonate and bicarbonate and for water autoionization/recombination, but order 10s for interconversion between bicarbonate and carbon dioxide. Bulk reaction phenomena can only be resolved with timesteps on the order of the fastest reaction–therefore, kinetic constants in both directions for carbonate to bicarbonate were slowed by a factor of 10^7 to order 1s–preserving two distinct timescales separated by an order of magnitude while maintaining the overall equilibrium and enabling the solver to progress in reasonable timesteps. Water dissociation and recombination is set implicitly by COMSOL to enforce the electroneutrality condition, and therefore did not require adjustment as a rate-limited reaction.

In the catalyst layer, the Secondary Current Distribution interface is applied to account for the hydrogen evolution reaction (HER) and (bi)carbonate formation. The model incorporates both ohmic and electrode polarization processes within the Secondary Current Distribution,

while the Transport of Diluted Species interface considers concentration distribution, fluid dynamics, as well as ion migration and diffusion. When modelling electrode kinetics in electrochemical systems (e.g., HER on RuO_2 or CER on DSA electrodes), the Butler-Volmer equation and charge transfer parameters are critical. Literature confirms the HER on RuO_2-based electrodes and CER on DSA electrodes exhibits a charge transfer coefficient of $\alpha \approx 0.5$[3-5]. The inlet concentration of dissolved CO_2 concentration was set to approximately 22.4 mM. Below is a summary of parameters for electrode reaction.

Table S2: Assumed Butler-Volmer and charge transfer parameters for the electrode models.

Parameter	**HER (A-RuO_x/Ti)**	**CER (DSA)**
α	0.5	0.5
i_0	0.1 A/m^2	1 A/m^2
E_0	-0.126 V vs RHE	1.48 V vs RHE

It should be noted that this simplified formulation assumes a constant exchange current density, but the thermodynamic basis of the Butler-Volmer model predicts dependence on the local activities of participating species.

Energy Consumption

The electrical energy per mole of captured CO_2 can be estimated from the cell voltage and electron utilization. Since 1 eV per electron = 96.49 kJ mol^{-1} (reflecting the Faraday constant, F = 96,485 C mol^{-1}), the ideal energy per mole is:

$$E_{\text{ideal}} = U \times 96.49 \text{ kJ mol}^{-1},$$

where U is the cell voltage in volts. Accounting for electron utilization via the ε_{CO_2} factor (electron efficiency), the minimum energy requirement becomes:

$$E = U \times 96.49/\varepsilon_{CO_2} \text{ kJ mol}_{CO2}^{-1}.$$

For instance, substituting U = 2.43 V and ε_{CO_2} = 1.31 (at 50 mA cm^{-2}):

$$E = 2.43 \times 96.49/\ 1.31 = 179 \text{ kJ mol}_{CO2}^{-1}$$

Techno-Economic Analysis

To assess the economic potential of electrochemical CO_2 capture via saline-water electrolysis, we performed a techno-economic analysis (TEA) following a modified framework from prior reports[6-9]. The base case reflects 90% CO_2 capture efficiency at a current density of 150 mA cm^{-2}, using an A-RuO_x/Ti cathode and a DSA anode. Assuming a capture rate of 1,000 kg_{CO2} day^{-1} and 350 operating days per year. For stand-alone CO_2 capture and $NaHCO_3$ production facilities, the techno-economic analysis now comprehensively accounts for three primary cost components: (1) saline water supply system, encompassing intake pumping, pretreatment, and transport infrastructure; (2) CO_2 capture unit, including capital investment and installation of the electrolysis system, operational electricity consumption for electrolysis, and routine maintenance; (3) product recovery system, covering the purification and processing of solid $NaHCO_3$.

1. Cost of saline water supply system

The capital and operating costs for saline water intake, pretreatment, and pumping align with standard cost structures used in seawater desalination plants. Capital expenditure for intake and pretreatment is calculated using an established correlation for integrated seawater intake-pretreatment systems. This widely adopted model, calibrated in 1995 U.S. dollars, has been extensively validated in desalination engineering literature[10-12]:

$$C_{SWIP} = 12659.84 Q_W^{0.8}$$

where Q_W is the flow rate of the water feed

Centrifugal pumps are used to supply pretreated saline water to the electrolysis system. The purchase cost of a centrifugal pump (C_{pump}) is estimated using the following cost function:

$$C_{pump} = F_m F_{pr} (Base\ cost)$$

$$Base\ cost = 844.31 Q_p^{0.3726}$$

where F_m and F_{pr} are the material adjustment factor and pressure adjustment factor, respectively. Stainless steel, with an F_m of 2.4, is the most commonly used material for seawater pumps. F_{pr} is taken as 1 for the pump. Q_p is the capacity of the centrifugal pump in $m^3\ h^{-1}$.

The total CapEx for saline water intake, pretreatment, and pumping is calculated as the sum of the individual cost functions, multiplied by a factor of 1.2 to account for indirect costs.

$$C_{CapEx} = 1.2(C_{SWIP} + C_{pump})$$

The OpEx include electricity, insurance, operation and maintenance (O&M), and labor, and are expressed as:

$$C_{OpEx} = C_{electricity} + C_{maintenance} + C_{labor} + C_{insurance}$$

$$C_{electricity} = P_p \times 24 \times C_e$$

$$C_{O\&M} = 0.01 \times C_{apEx}$$

$$C_{insurance} = 0.005 \times C_{CapEx}$$

Where P_p represents the pump power required for seawater intake, pretreatment, and delivery, C_e denotes the electricity cost, assumed to \$0.05 kWh^{-1}, annual labor costs are estimated at \$50000.

At the industrial scale, the equipment configuration–including the size and number of CO_2 capture units–has been systematically designed to meet operational requirements. The system is designed to capture 1 ton of CO_2 per day at a Faradaic efficiency of 90%, with a total daily brine consumption of 900 kg across the anode and cathode compartments, corresponding to a stoichiometric flow rate of approximately 0.04 $m^3\ h^{-1}$. However, to ensure effective CO_2 dissolution and maintain stable electrolyzer operation without running dry, a practical recirculation flow rate of 5 $m^3\ h^{-1}$ was adopted for sizing key components such as the electrolyzer and absorption tank. This reflects real-world engineering margins and operational reliability considerations. All cost estimates have been annualized and discounted to the construction year using a 5% discount rate, incorporating depreciation and other relevant financial parameters to reflect the full lifecycle economics over the assumed 20-year amortization period. The cost of saline water supply system is estimated at \$158 t_{CO2}^{-1}. For an CO_2 capture system co-located with a seawater desalination facility, the costs associated with seawater intake, pretreatment, and pumping are assumed to be covered by the desalination plant.

2. Cost of CO_2 capture unit

The total current required is:

$$Total\ current = 1000 * \frac{kg}{day} * \frac{day}{24\ h} * \frac{h}{3600\ s} * \frac{kmol}{44\ kg} * 2e^- * 96485 * \frac{C}{mol} * \frac{1}{90\%}$$

$$= 56400.23\ A$$

The required electrolyzer area at 150 mA cm^{-2} is:

$$Total\ electrolyzer\ area = \frac{56400.23\ A}{0.15\ A\ cm^{-2}} * \frac{m^2}{10^4 cm^2} = 37.60\ m^2$$

With a cell voltage of 2.8 V at 150 mA cm^{-2}, the electrical power is:

$$Power = voltage * 56400.23\ A * \frac{W}{10^3 kW} = 157.92\ kW$$

(1) Electrolyzer cost

Using DOE H2A stack cost \$250.25 kW^{-1} at a reference condition of 175 mA cm^{-1} and 1.75 V, the stack capital is estimated as:

$$Electrolyzer\ cost = electrolyzer\ area * Reference\ cost * Reference\ current\ density * \frac{A}{1000\ mA} * \frac{kW}{1000\ W} * Reference\ voltage * \frac{10^4 cm^2}{m^2}$$

$$= 37.60\ m^2 * \frac{\$250.25}{kW} * 175\ mA\ cm^{-2} * \frac{A}{1000\ mA} * \frac{kW}{1000\ W} * 1.75\ V * \frac{10^4 cm^2}{m^2} = \$28816.29$$

Annualization uses a capital-recovery factor (CRF) with i = 5% and lifetime = 20 years.

$$CRF_{electrolyzer} = \frac{i(1+i)^{year}}{(1+i)^{year} - 1} = \frac{0.05 * 1.05^{20}}{1.05^{20} - 1} 0.0802$$

Thus, the stack cost per ton CO_2 is

$$Electrolyzer\ cost_{per\ ton\ CO_2} = \$28816.29 * \frac{0.0802}{350} = \$6.6$$

(2) Electricity cost

Assuming \$0.05 kWh^{-1}, the electricity cost per captured ton (1 ton day^{-1} base) is:

$$Electricity\ cost_{per\ ton\ CO_2} of\ \text{electrolysis} = 157.92\ kW * 24\ hr * \frac{\$0.05}{kWh} = \$190$$

(3) Balance of plant (BoP) cost

Assuming BoP equals 50% of total capital (stack) cost:

$$BOP\ cost = Electrolyzer\ cost * 50\% = \$6.6 * 50\% = \$3.3$$

(4) Stack replacement cost

Assuming 30% of installed stack cost every 7 years:

$$Stack\ replacement\ cost = \$28816.29 * \frac{0.3}{7 * 350} = \$3.5$$

(5) Other operational costs

We assume labor & maintenance = 2.5% of stack cost per ton and pumping (CapEx + OpEx) $\approx$ 5% of stack cost, totaling 7.5%:

$$Other\ cost_{per\ ton\ CO_2} = Electrolyzer\ cost * (2.5\% + 5\%) = \$6.6 * 7.5\% = \$0.49$$

Thus, the cost of CO_2 capture unit is:

$$Capture\ unit\ cost_{per\ ton\ CO_2} = \$6.6 + \$190 + \$3.3 + \$3.5 + \$0.49 = \$204$$

3. Potential profit from co-products

We assume the reference prices of H_2, Cl_2, and $NaHCO_3$ solid are \$4500 ton^{-1}, \$49 ton^{-1}, and \$450 ton^{-1}, respectively. The corresponding quantity of H_2, Cl_2, and pure $NaHCO_3$ is calculated according to:

$$Profit\ of\ H_2 = 56400.23A * \frac{1}{2e^- * 96485 \frac{C}{mol}} * \frac{0.002\ kg}{mol} * \frac{86400\ s}{day} * \frac{\$4500}{1000\ kg} * 90\%$$

$$= \$204$$

$$Profit\ of\ Cl_2 = 56400.23A * \frac{1}{2e^- * 96485 \frac{C}{mol}} * \frac{0.071\ kg}{mol} * \frac{86400\ s}{day} * \frac{\$49}{1000\ kg} * 90\%$$

$$= \$79$$

The conversion efficiency of $NaHCO_3$ is calculated at 85%. Potential profit from selling $NaHCO_3$:

$$NaHCO_3\ mass\ flow\ rate = \frac{1000000 \frac{g}{day}}{44 \frac{g}{mol}} * \frac{0.084\ kg}{mol} * 85\% = 1623 \frac{kg}{day}$$

Through continuous electrolyte circulation, our capture system achieves a saturated $NaHCO_3$ solution. Based on established industrial purification methods for such streams and accounting for the energy cost of water evaporation and capital equipment, we estimate the cost of crystallizing and drying the solid $NaHCO_3$ to be approximately \$400 per ton, and assuming an 80% recovery rate of $NaHCO_3$.

$$Profit\ of\ NaHCO_3 = 1.623 * (\$450 - \$400) * 80\% = \$65$$

Total potential revenue (base):

$$Overall\ profit_{per\ ton\ CO_2} = \$204 + \$79 + \$65 = \$348$$

Supplementary Figures

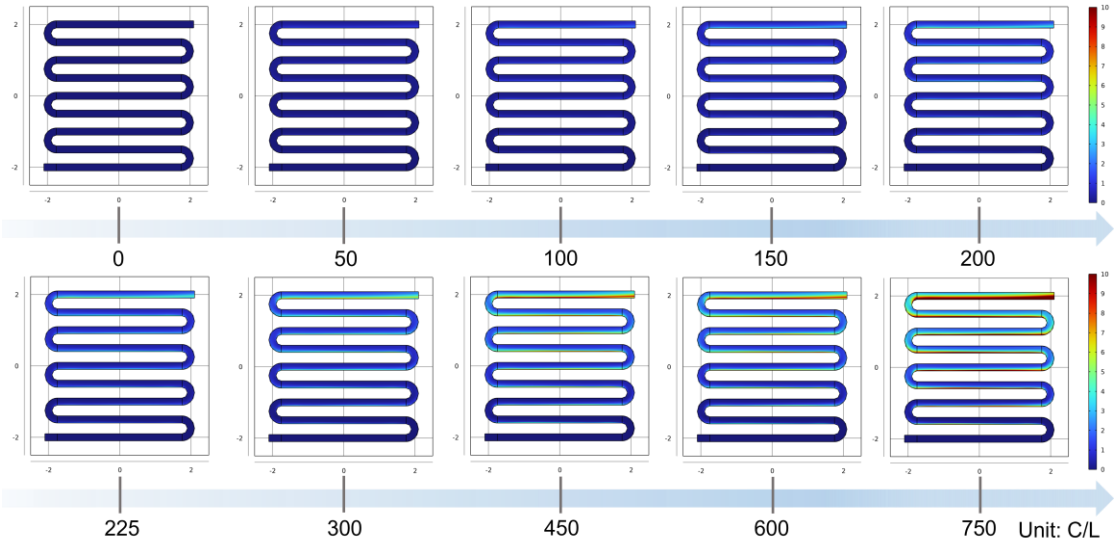

Fig. S2 COMSOL-simulated pH profiles in the designed flow channel as a function of total applied charge (without CO_2 input).

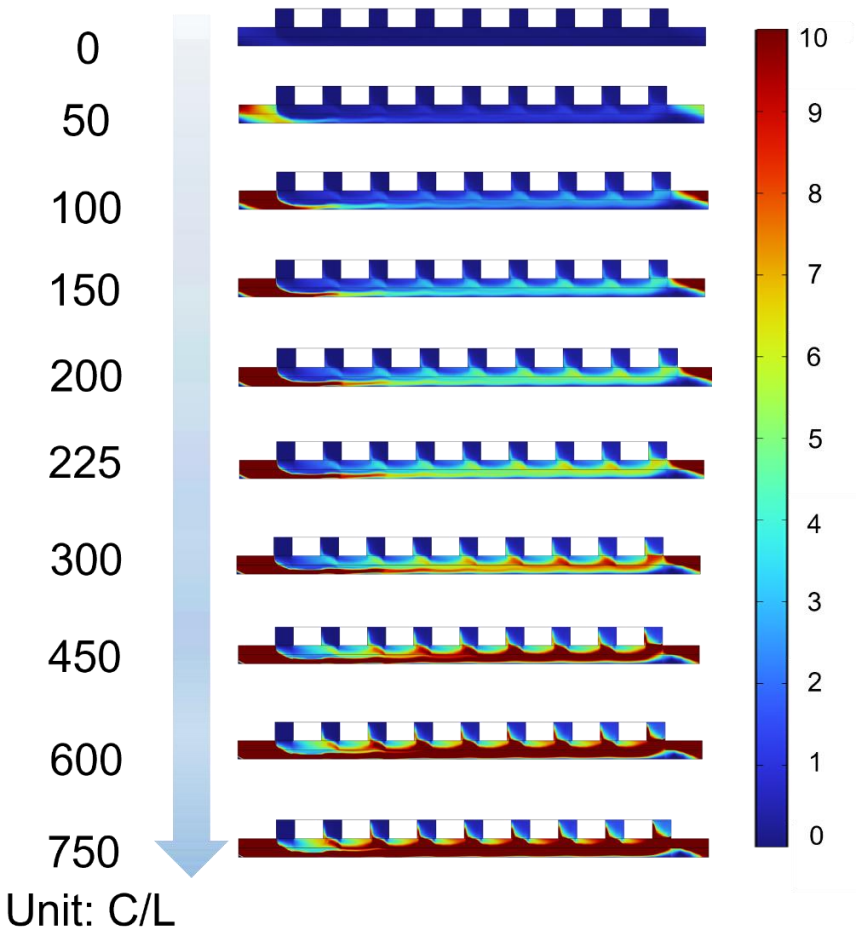

Fig. S3 COMSOL-simulated pH profiles in the hydrodynamic boundary-layer as a function of total applied charge (without CO_2 input).

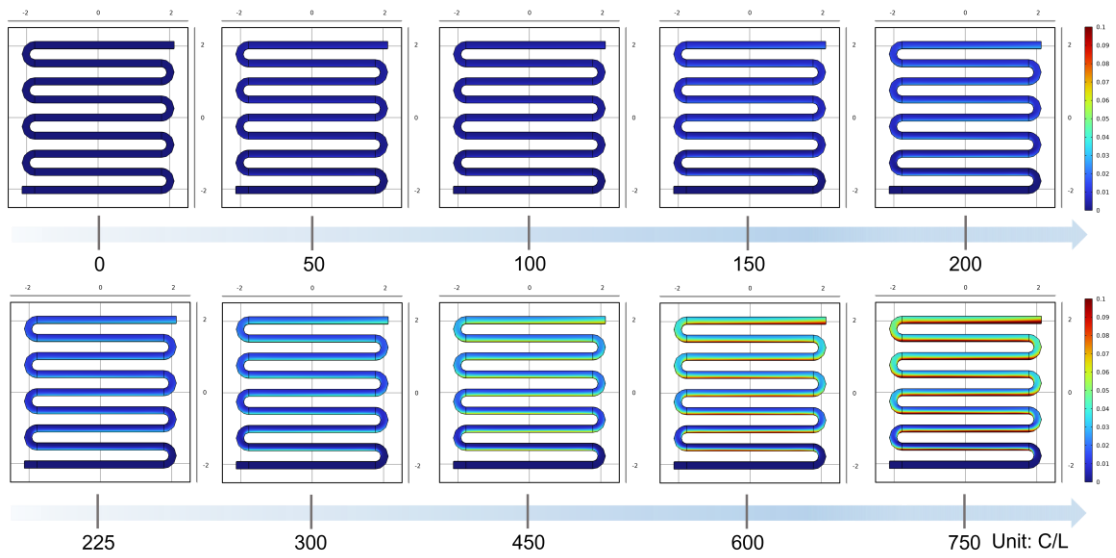

Fig. S4 COMSOL-simulated pH profiles in the designed flow channel as a function of total applied charge (with CO_2 input).

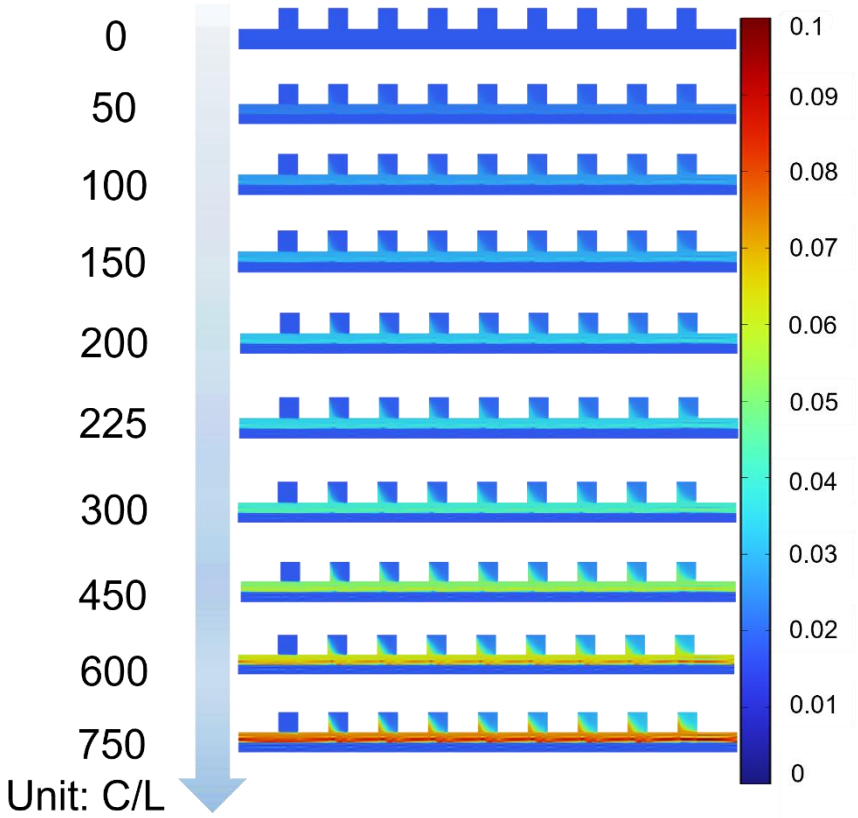

Fig. S5 COMSOL-simulated pH profiles in the hydrodynamic boundary-layer as a function of total applied charge (with CO_2 input).

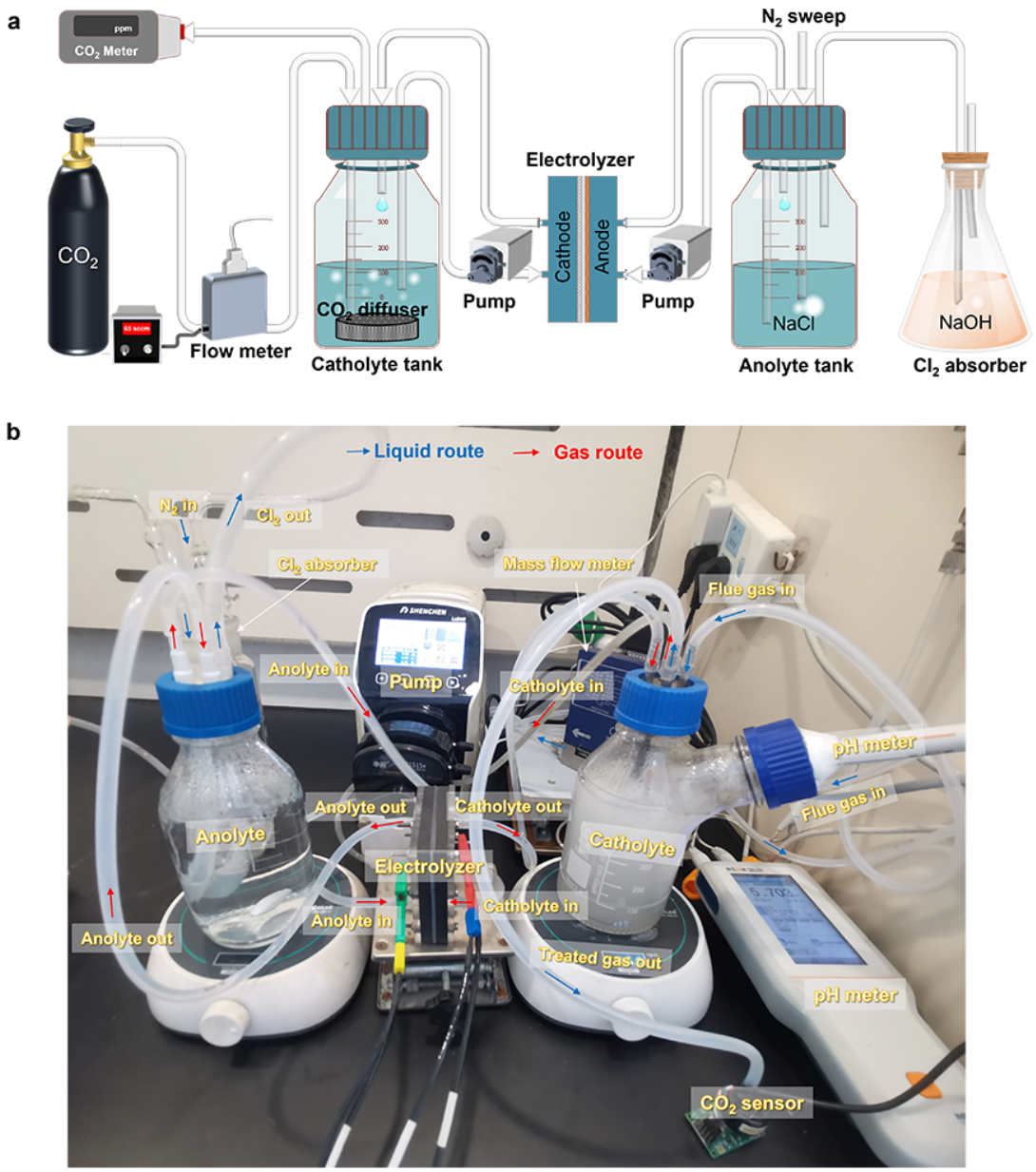

Fig. S6 (a) Schematic of CO_2 capture and conversion system. (b) Photograph of the saline-water electrolysis system used for CO_2 capture.

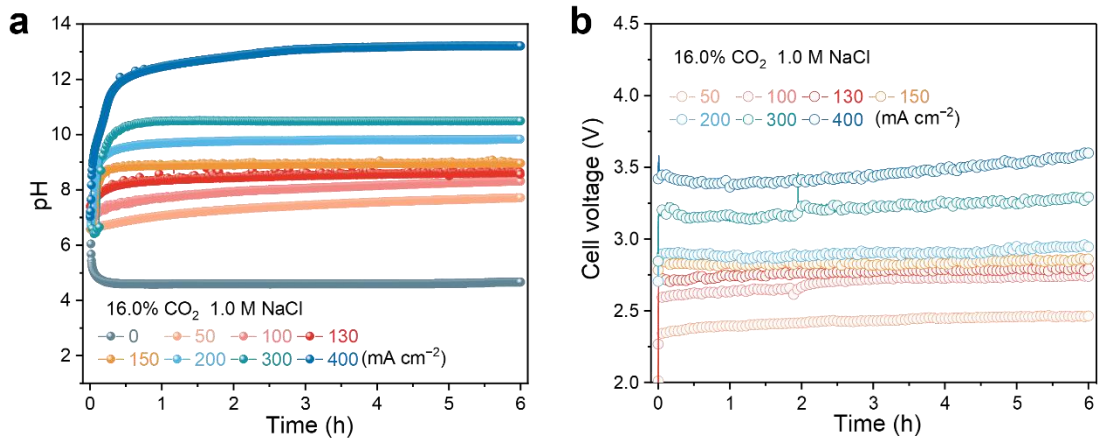

Fig. S7 (a) pH profiles and (b) cell voltage of the saline-water electrolysis system at different current densities. Tests employed 1.0 M NaCl (500 mL catholyte and 500 mL anolyte) circulated at 200 mL min^{-1}. All measurements were performed at room temperature under a constant simulated flue gas flow rate of 65 sccm.

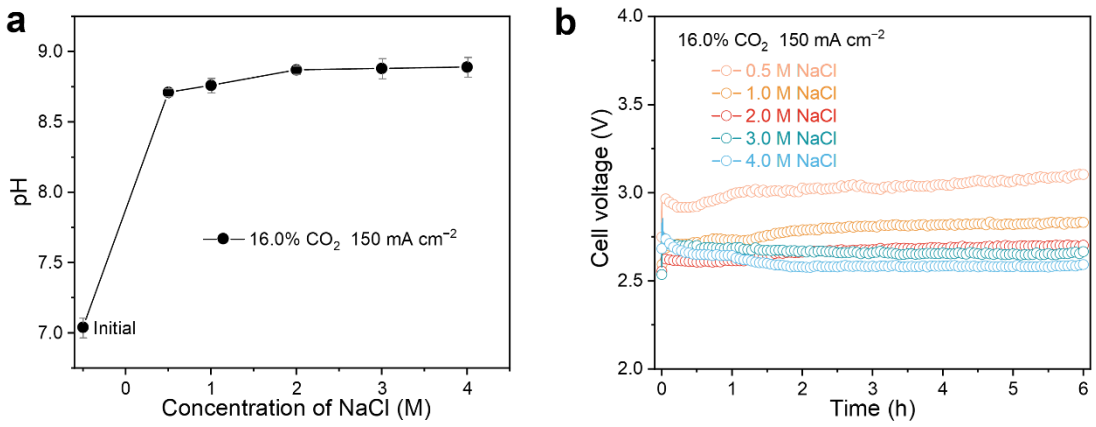

Fig. S8 (a) pH profiles and (b) cell voltage of the saline-water electrolysis system as a function of NaCl concentration at a fixed current density of 150 mA cm^{-2}. All experiments were conducted at room temperature with a simulated flue gas flow rate of 65 sccm.

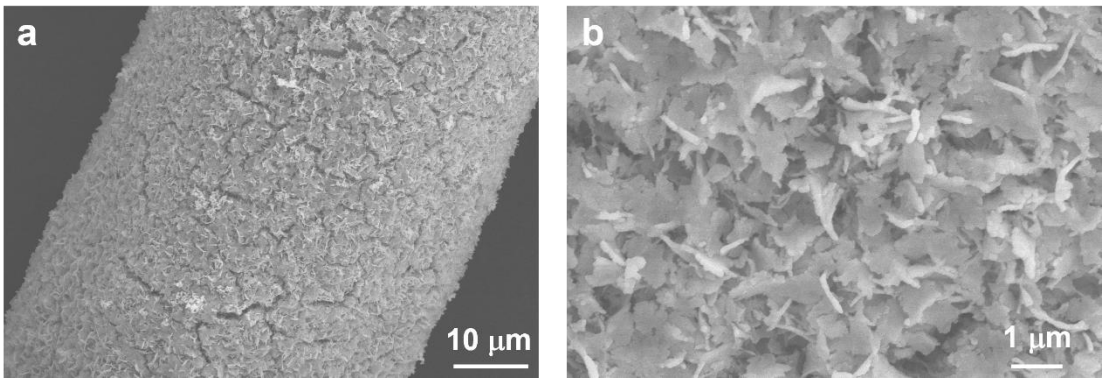

Fig. S9 Morphological characterization of A-RuO_x/Ti: (a) Low magnification and (b) high magnification SEM images of A-RuO_x/Ti celectrode.

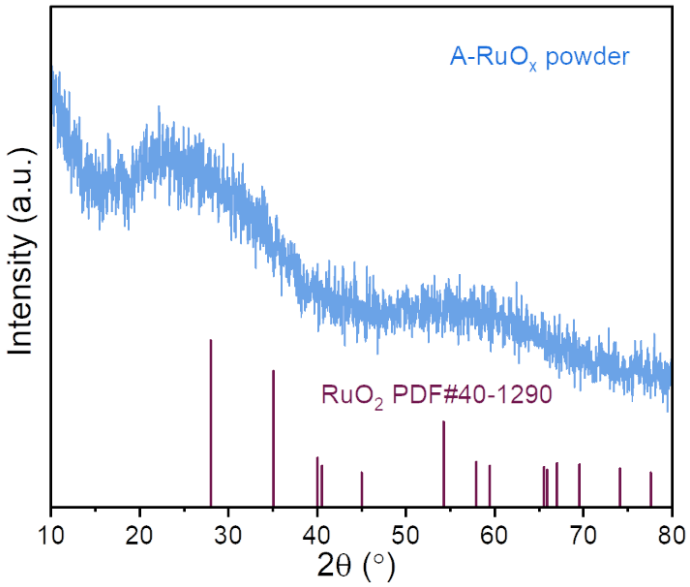

Fig. S10 XRD pattern of A-RuO_x powder scraped from the titanium mesh substrate.

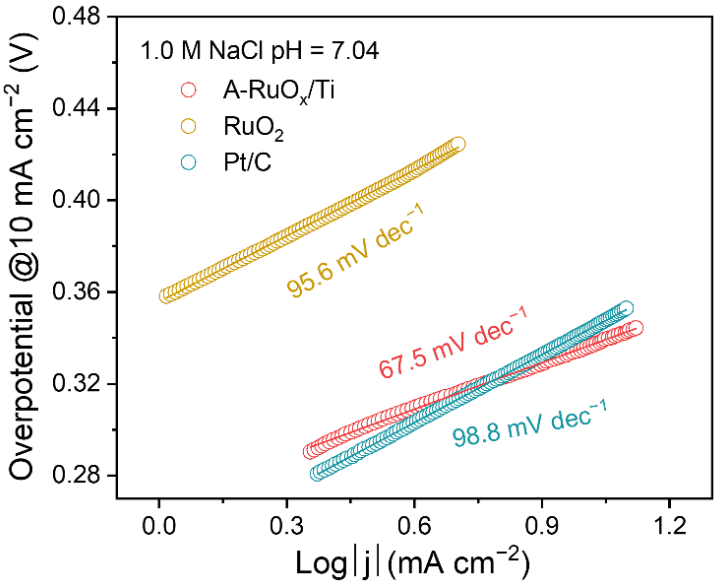

Fig. S11 Tafel plots derived from LSV curves for A-RuO_x/Ti, RuO_2, and Pt/C.

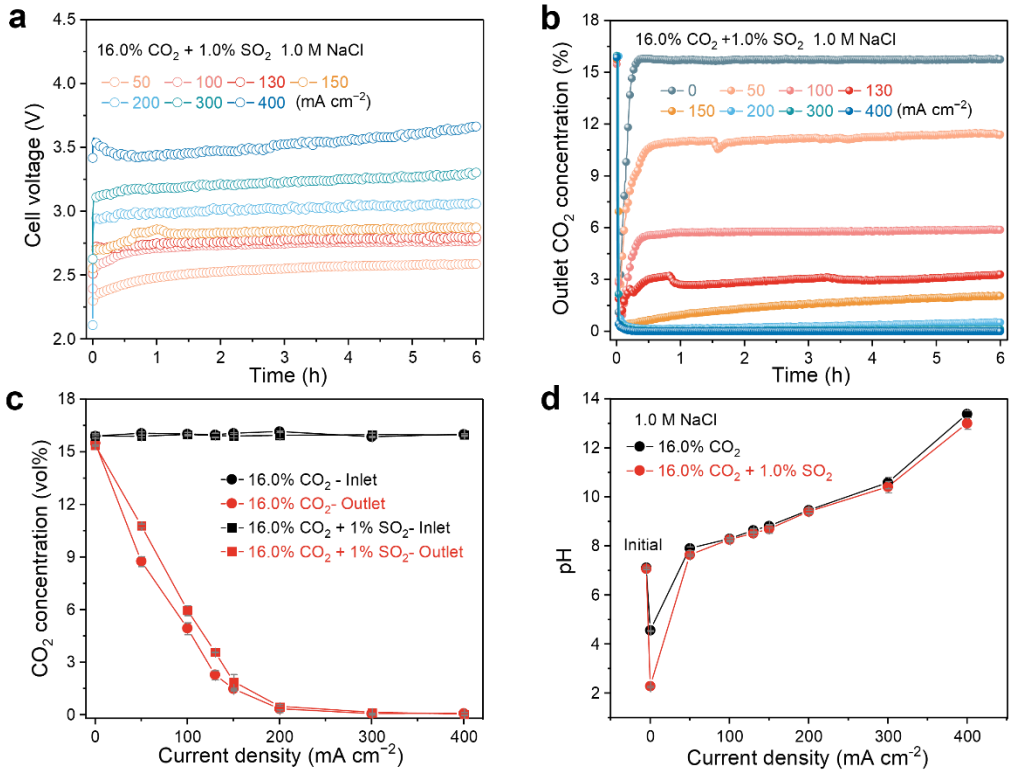

Fig. S12 CO_2 capture performance with SO_2-containing flue gas using A-RuO_x/Ti. (a) Cell voltage and (b) outlet CO_2 concentration at various current densities under SO_2-containing flue gas (16.0% CO_2, 1.0%SO_2, 5.6% O_2, and 77.4% N_2; 65 sccm). (c) Comparison of outlet CO_2 concentration and (d) final catholyte pH for SO_2-containing versus SO_2-free feeds in saline water electrolysis system.

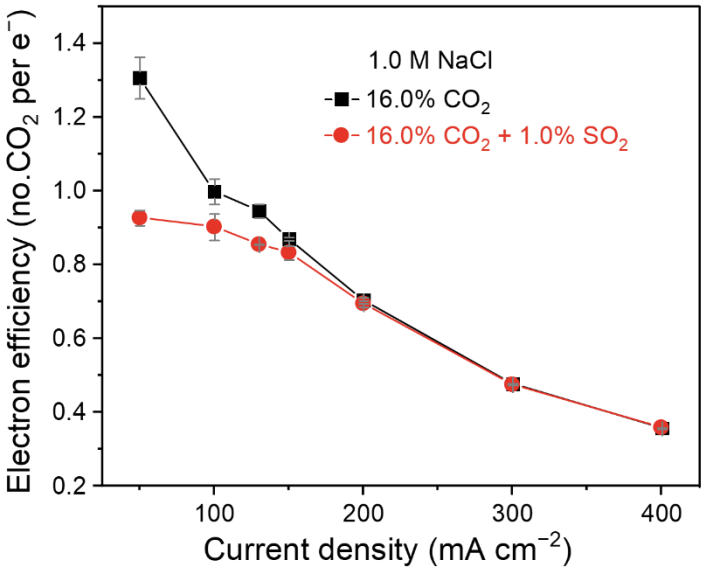

Fig. S13 Effect of SO_2 on electron efficiency in the saline water electrolysis system at different current densities.

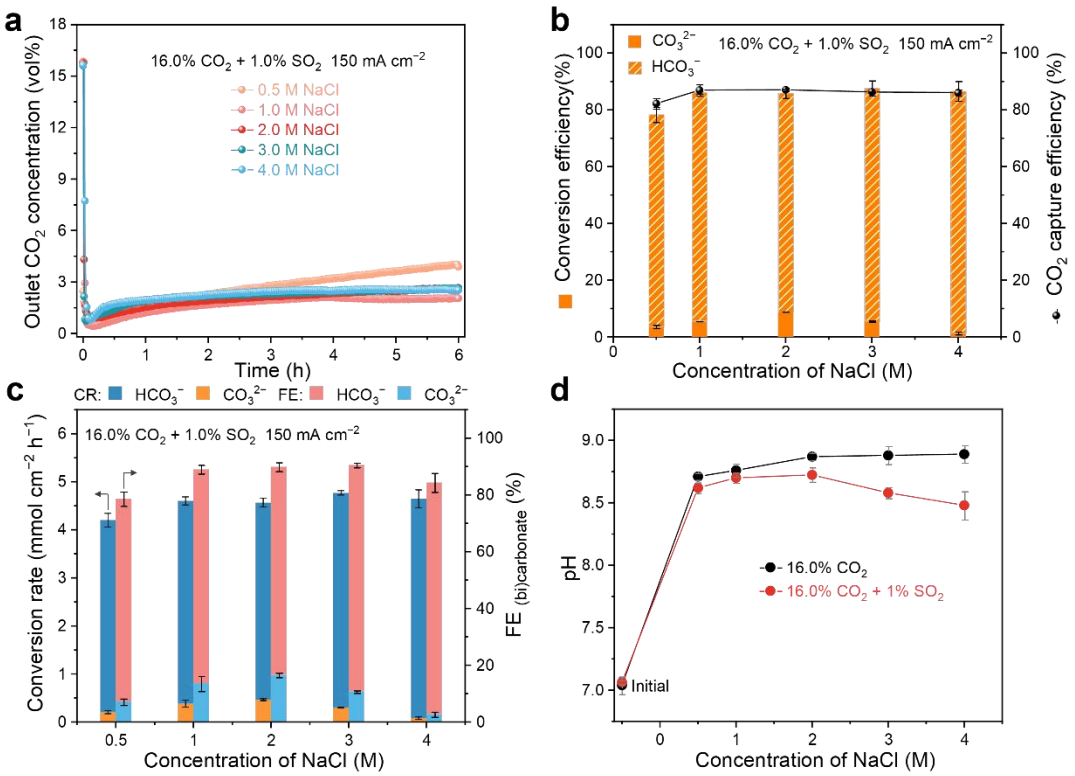

Fig. S14 Performance evaluation of CO_2 capture from SO_2-containing flue gas using A-RuO_x/Ti. The change of outlet CO_2 concentration (a), corresponding CO_2 capture efficiency and $NaHCO_3/Na_2CO_3$ conversion efficiency (b), $NaHCO_3/Na_2CO_3$ conversion rate and Faradaic efficiency (c) of the saline-water electrolysis system with different concentration of NaCl and fixed the current density at 150 mA cm^{-2}, the SO_2-containing flue gas (16.0% CO_2, 1.0%SO_2, 5.6% O_2, and 77.4% N_2) as the gas input. (d) The comparison of final pH between SO_2-containing and SO_2-free flue gas as input gas in the saline-water electrolysis system. All tests were performed at room temperature operating with a gas flow rate of 65 sccm.

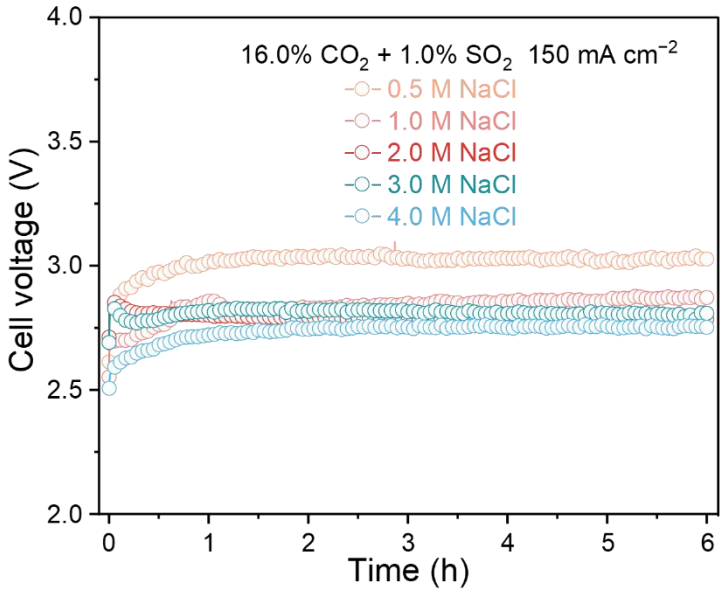

Fig. S15 Cell voltage of the saline water electrolysis system as a function of NaCl concentration at a fixed current density of 150 mA cm^{-2}. Measurements were performed with SO_2-containing flue gas (16.0% CO_2, 1.0%SO_2, 5.6% O_2, and 77.4% N_2) at a total flow rate of 65 sccm.

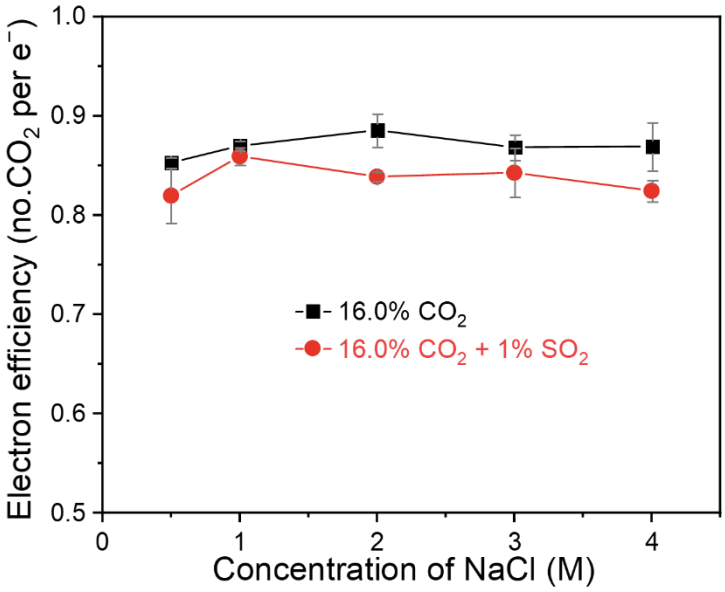

Fig. S16 Effect of SO_2 on electron efficiency in saline water electrolysis system under different concentration of NaCl.

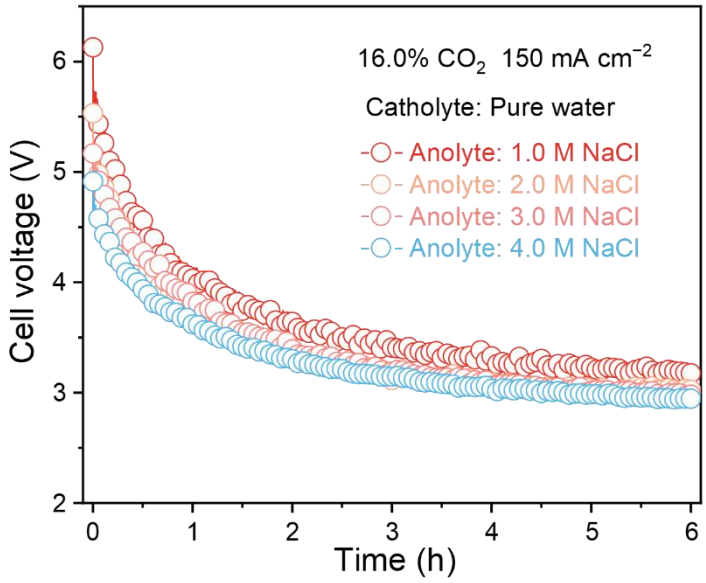

Fig. S17 Cell voltage of the pure water catholyte system as a function of anolyte NaCl concentration at a fixed current density of 150 mA cm^{-2}. Simulated flue gas (16.0% CO_2, 5.6% O_2, and 78.4% N_2) was supplied at 65 sccm.

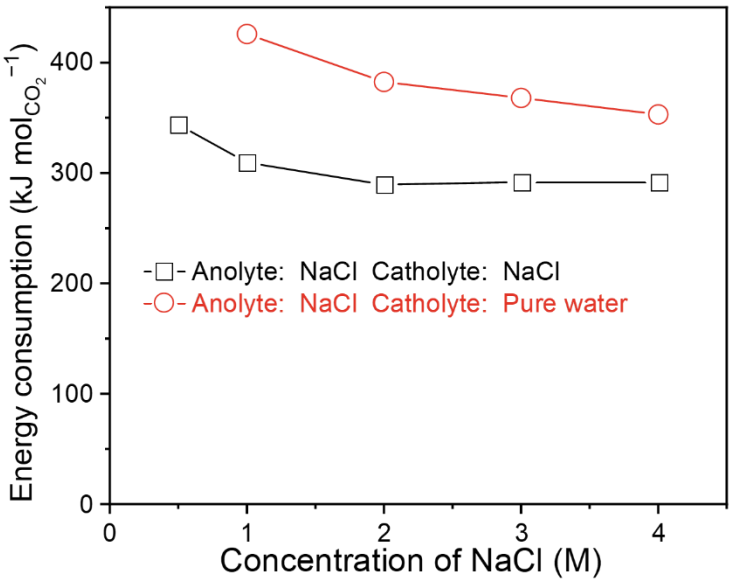

Fig. S18 Comparative energy consumption of the saline water electrolysis system and the pure water catholyte system as a function of anolyte NaCl concentration at a fixed current density of 150 mA cm^{-2}. Simulated flue gas (16.0% CO_2, 5.6% O_2, and 78.4% N_2) was supplied at 65 sccm.

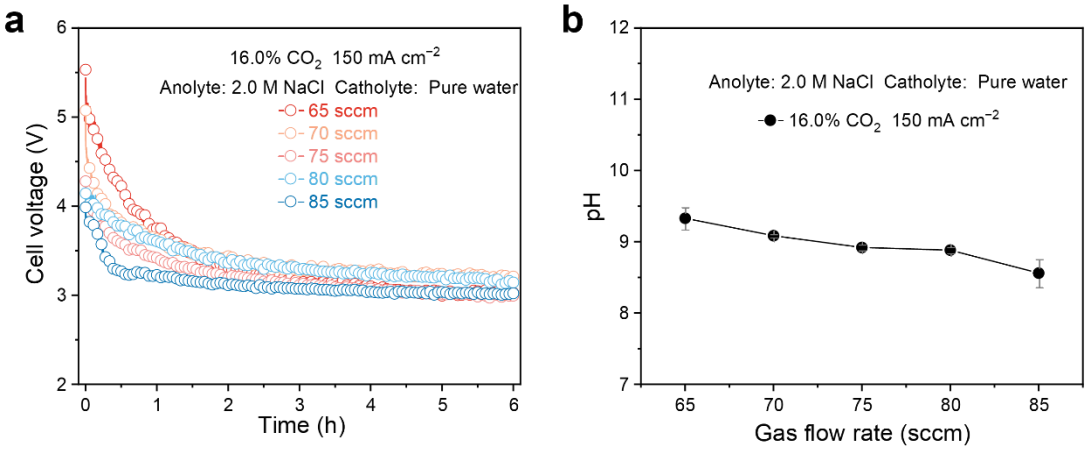

Fig. S19 (a) Cell voltage and (b) catholyte pH of the pure water system as a function of gas feed rate at a fixed current density of 150 mA cm^{-2}. Simulated flue gas (16.0% CO_2, 5.6% O_2, and 78.4% N_2) was supplied at the indicated total flow rates.

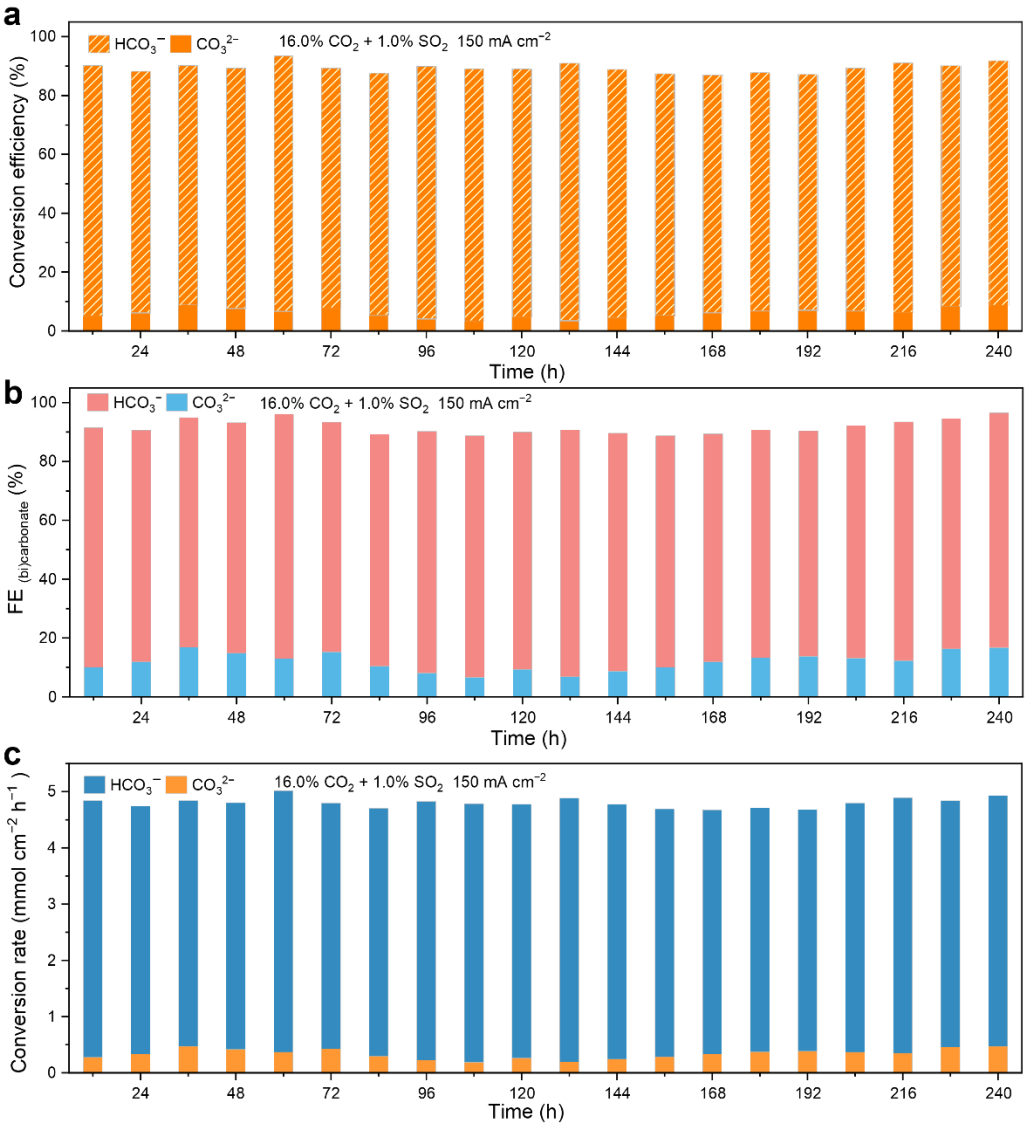

Fig. S20 Long-term stability of the pure water catholyte system with SO_2-containing flue gas. Panels show (a) $NaHCO_3/Na_2CO_3$ conversion efficiencies, (b) total Faradaic efficiencies, and (c) $NaHCO_3/Na_2CO_3$ conversion rates over time. Experiments were conducted at 150 mA cm^{-2} (total current 750 mA) with a gas flow rate of 65 sccm; the anolyte was 3 L of 2.0 M NaCl replaced every 48 h, and the catholyte was 500 mL of deionized water refreshed every 12 h.

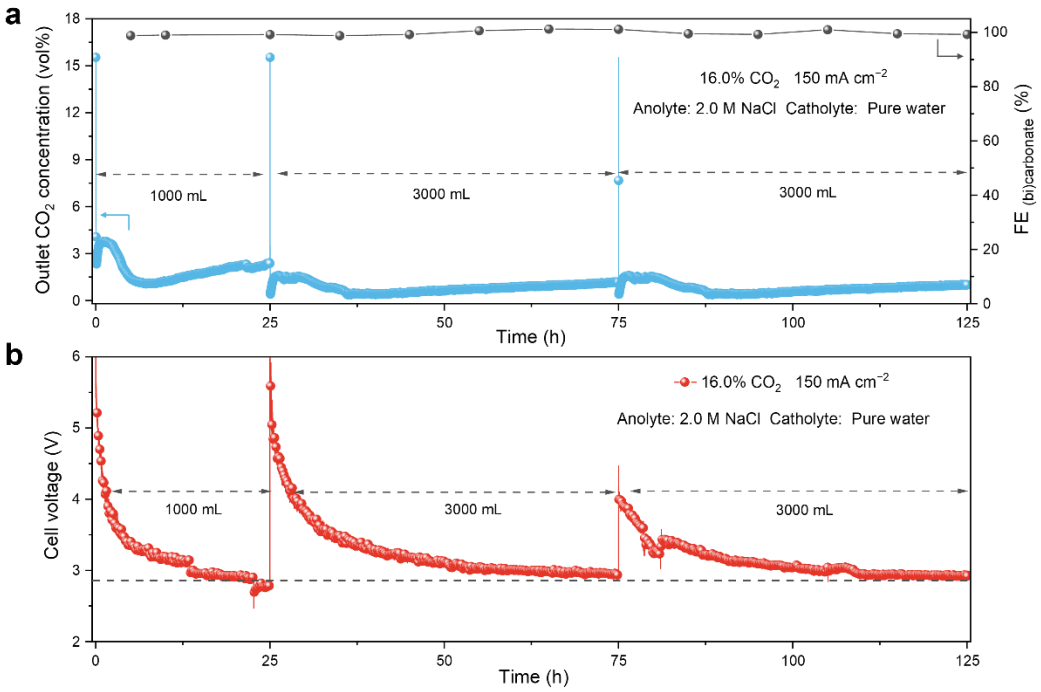

Fig. S21 Stability of the pure water catholyte system with SO_2-free flue gas. (a) Outlet CO_2 concentration and total Faradaic efficiency over time. (b) Cell voltage. Experiments were conducted at 150 mA cm^{-2} (total current 750 mA) with simulated SO_2-free flue gas at 65 sccm. Anolyte: 2.0 M NaCl; catholyte: pure water. Electrolyte volumes were 1,000 mL each in the first cycle and 3,000 mL in subsequent cycles.

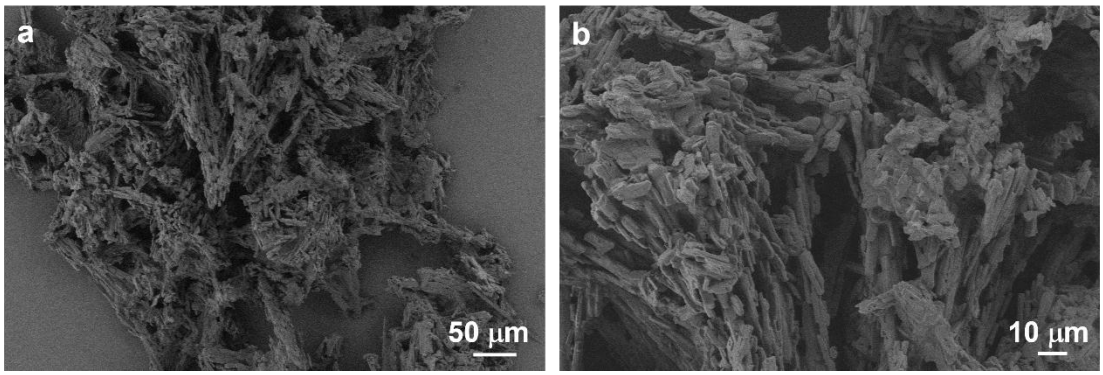

Fig. S22 Morphological characterization of solid product $NaHCO_3$. (a) Low magnification and (b) high magnification SEM images.

Supplementary Tables

Table S3: The S content in the catholyte obtained from experiments at different current densities.

Current density (mA cm^{-2})	Catholyte S Content (mol)
0	0.00776
50	0.00792
100	0.00816
130	0.00838
150	0.00846
200	0.00852
300	0.00880
400	0.00908

Table S4: The S content in the catholyte obtained from experiments at different NaCl concentration.

Catholyte NaCl concentration (M)	Catholyte S Content (mol)
0.5	0.00841
1.0	0.00846
2.0	0.00852
3.0	0.00998
4.0	0.0109

Table S5: The average final content of Na^+, CO_3^{2-}, and HCO_3^- in the catholyte obtained from pure water system under varying anolyte NaCl concentration.

Anolyte NaCl concentration (M)	**Catholyte Na^+ content (mol)**	**Catholyte CO_3^{2-} content (mol)**	**Catholyte HCO_3^- content (mol)**
Pure water	0	0	0
1.0	0.162	0.0254	0.113
2.0	0.186	0.0244	0.118
3.0	0.193	0.0236	0.120
4.0	0.228	0.0240	0.119

Table S6: The average final content of Na^+, CO_3^{2-}, and HCO_3^- in the catholyte obtained from pure water system under varying input gas flow rate.

Input gas flow rate (sccm)	**Catholyte Na^+ content (mol)**	**Catholyte CO_3^{2-} content (mol)**	**Catholyte HCO_3^- content (mol)**
65	0.186	0.0244	0.118
70	0.188	0.0155	0.138
75	0.173	0.0131	0.144
80	0.184	0.00989	0.149
85	0.186	0.00614	0.156

Table S7: The content of Na and S in the catholyte obtained from the stability test of our pure water system.

Time (h)	Catholyte Na^+ Content (mol)	Catholyte S Content (mol)
12	0.282	0.0166
24	0.269	0.0164
36	0.303	0.0169
48	0.239	0.0175
60	0.355	0.0178
72	0.273	0.0154
84	0.296	0.0172
96	0.289	0.0177
108	0.276	0.0179
120	0.306	0.0185
132	0.300	0.0182
144	0.266	0.0174
156	0.283	0.0169
168	0.266	0.0167
180	0.283	0.0164
192	0.292	0.0169
204	0.314	0.0186
216	0.321	0.0193
228	0.317	0.0174
240	0.259	0.0163

Table S8: Comparison of representative carbon capture technologies.

Method	Carbon capture mechanism	CO_2 source	SO_2/O_2 resistivity	Current density (mA cm^{-2})	Current efficiency (%)	Energy kJ mol_{CO2}^{-1}	Output	Reference
Electrolysis	**HER/CER**	**16.0% CO_2**	**Yes**	**50-300**	**~87-99**	**87-562$_e$**	**$NaHCO_3$**	**This work**
Electrolysis	OER/ORR	13.9% CO_2	Yes	0.5-500	~87-95	150-600$_e$	CO_2	9
BPMED	pH-swing by electrochemical water splitting	0.5 M $KHCO_3$	Yes	20-140	70-90	200-400$_e$ (desorption)	CO_2	13
				5-80	~90	148-325$_e$ (desorption)	CO_2	14
Electrodialysis	OER/HER	Pure CO_2 gas dissolved in DI water	Yes	1.5	~86	Not reported	$NaHCO_3$	15
Gas-Fed electrodialysis	OER/ORR	CO_2 gas (0–50% in O_2 gas)	Yes	20-30	~71	Not reported	$NaHCO_3$	16
Electrodialysis	pH-swing by electrochemical water splitting	10%CO_2	Yes	19.4	~87	~1770$_e$	$NaHCO_3$ + Na_2CO_3	17
EMAR	Electrochemically mediated amine regeneration	15% CO_2	No	2-12	~80	40-120e (desorption)	CO_2	18, 19
Redox-Active Quinone	Redox-active quinones in ionic liquid electrolyte	15%CO_2	No	~1	<100	50-200e	CO_2	20
Redox-Tunable sp^2-N	Redox-tunable nitrogen centers in ionic liquid electrolyte	18.5%CO_2	3%O_2	2	87	120$_e$	CO_2	21
		15%CO_2	5%O_2	2	82	156$_e$	CO_2	21
PCET	pH-swing by proton-coupled electron transfer	15%CO_2	No	40-150	<100	16-75$_e$*	CO_2	22
Amine Scrubbing	Concentrated MEA or PZ	12%CO_2	No	N.A.	N.A.	120-200$_{th}$*	CO_2	23
		12%CO_2	No	N.A.	N.A.	150-250$_{th}$*	CO_2	24

Note:The subscript “e” represents electrical energy and “th” represents thermal energy. *Estimated minimum energy consumption.

References

1 B. Ravela and M. Newvilleb, ATHENA, ARTEMIS, HEPHAESTUS: data analysis for X-ray absorption spectroscopy using IFEFFIT. *J. Synchrotron Radiat.*, 2005, **12**, 537-541.

2 Richard E. Zeebe, History of seawater carbonate chemistry, atmospheric CO_2, and ocean acidification. *Annu. Rev. Earth Planet. Sci.*, 2012, **40**, 141-165.

3 B. E. Conway, and B. V.Tilak, Interfacial processes involving electrocatalytic evolution and oxidation of H_2, and the role of chemisorbed H. *Electrochim. Acta*, 2002, **47**, 3571-3594.

4 J. K. Nørskov, T. Bligaard, A. Logadottir, J. R. Kitchin, J. G. Chen, S. Pandelov and U. Stimming, Trends in the exchange current for hydrogen evolution. *J. Electrochem. Soc.*, 2005, **152**, J23-J26.

5 K. S. Exner, Beyond the traditional volcano concept: overpotential-dependent volcano plots exemplified by the chlorine evolution reaction over transition-metal oxides. *J. Phys. Chem. C*, 2019, **123**, 16921-16928.

6 J. H. Lee, J. H. Lee, I. K. Park, and C. H. Lee, Techno-economic and environmental evaluation of CO_2 mineralization technology based on bench-scale experiments. *J. CO_2 Util*., 2018, **26**, 522-536.

7 H. Shin, K. U. Hansen, and F. Jiao, Techno-economic assessment of low-temperature carbon dioxide electrolysis. *Nat. Sustain.*, 2021, **4**, 911-919.

8 Y. F. Zhu, J. D. Wang, Y. Ou, J. Fuhrman, H. D. Ji, M. Lin, Y. D. Hu, K. C. Zuo, H. Z. Zhao, and Z. S. Zhang, Asymmetric electrosorption in a bio-inspired reactor enables energy efficient ocean carbon removal. *Angew. Chem. Int. Ed.*, 2025, e202515007.

9 P. Zhu, Z. Y. Wu, A. Elgazzar, C. X. Dong, T. U. Wi, F. Y. Chen, Y. Xia, Y. G. Feng, M. Shakouri, J. Y. Kim, Z. W. Fang, T. A. Hatton and H. T. Wang, Continuous carbon capture in an electrochemical solid-electrolyte reactor. *Nature*, 2023, **618**, 959-966.

10 Wan, C. F. and T.-S. Chung, Techno-economic evaluation of various RO+PRO and RO+FO integrated processes. *Appl. Energy*, 2018, 212, 1038-1050.

11 M. G. Marcovecchio, Pío A. Aguirre, and Nicolás J. Scenna, Global optimal design of reverse osmosis networks for seawater desalination: modeling and algorithm. *Desalination*, 2005, 184, 259-271.

12 F. Vince, F. Marechal, E. Aoustinand, and P. Bréant. Multi-objective optimization of RO desalination plants. *Desalination*, 2008, 222, 96-118.

13 M. D. Eisaman,. L. Alvarado,. D. Larner,. P. Wang and K. A. Littau, CO_2 desorption using high-pressure bipolar membrane electrodialysis. *Energy Environ. Sci.*, 2011, **4**, 4031-4037.

14 M. D. Eisaman, L. Alvarado, D. Larner, P. Wang, B. Garga and K. A. Littaua, CO_2 separation using bipolar membrane electrodialysis. *Energy Environ. Sci.*, 2011, **4**, 1319-1328.

15 S. Dara, M. Lindstrom, J. English, A. Bonakdarpour, B. Wetton and D. P. Wilkinson, Conversion of saline water and dissolved carbon dioxide into value-added chemicals by electrodialysis. *J. CO_2 Util*., 2017, **19**, 177-184.

16 S. Dara, A. Bonakdarpour, M. Ho, R. Govindarajana and D. P. Wilkinson, Conversion of saline waste-water and gaseous carbon dioxide to (bi)carbonate salts, hydrochloric acid and desalinated water for on-site industrial utilization. *React. Chem. Eng*., 2019. **4**, 141-150.

17 J. Mustafa, A. H. Al-Marzouqi, N. Ghasem, M. H. El-Naas and B. Van der Bruggen, Electrodialysis process for carbon dioxide capture coupled with salinity reduction: A statistical and quantitative investigation. *Desalination*, 2023. **548**, 116263.

18 M. Wang, S. Hariharan, R. A. Shaw and T. A. Hatton, Energetics of electrochemically mediated amine regeneration process for flue gas CO_2 capture. *Int. J. Greenhouse Gas Control*, 2019, **82**, 48-58.

19 M. Wang, H. J. Herzog and T. A. Hatton, CO_2 capture using electrochemically mediated amine regeneration. *Ind. Eng. Chem. Res.*, 2020, **59**, 7087-7096.

20 K. M. Diederichsen, Y. Liu, N. Ozbek, H. Seo, T. A. Hatton, Toward solvent-free continuous-flow electrochemically mediated carbon capture with high-concentration liquid quinone chemistry. *Joule*, 2022, **6**, 221-239.

21 X. Li, X. Zhao, Y. Liu, T. A. Hatton and Y. Liu, Redox-tunable Lewis bases for electrochemical carbon dioxide capture. *Nat. Energy*, 2022, **7**, 1065-1075.

22 S. Jin, M. Wu, R. G. Gordon, M. J. Aziz and D. G. Kwabi, pH swing cycle for CO_2 capture electrochemically driven through proton-coupled electron transfer. *Energy Environ. Sci.*, 2020, **13**, 3706-3722.

23 Y. J. Lin, and G. T. Rochelle, Approaching a reversible stripping process for CO_2 capture. *Chem. Eng. J.*, 2016, **283**, 1033-1043.

24 Lin, Y. J., Chen, E., & Rochelle, G. T. Pilot plant test of the advanced flash stripper for CO_2 capture. *Faraday Discuss.* **192**, 37-58 (2016).